Understanding the metabolic fate and assessing the biosafety of MnO nanoparticles by metabonomic analysis

2013 Nanotechnology 24 455102

(http://iopscience.iop.org/0957-4484/24/45/455102)

Nanotechnology **24** (2013) 455102 (14pp) doi:10.1088/0957-4484/24/45/455102

Understanding the metabolic fate and assessing the biosafety of MnO nanoparticles by metabonomic analysis

Jinquan Li[1], Zhenghuan Zhao[2], Jianghua Feng[1], Jinhao Gao[2] and Zhong Chen[1]

[1] Fujian Provincial Key Laboratory of Plasma and Magnetic Resonance, State Key Laboratory of Physical Chemistry of Solid Surfaces, Department of Electronic Science, Xiamen University, Xiamen 361005, People's Republic of China
[2] The Key Laboratory for Chemical Biology of Fujian Province and Department of Chemical Biology, College of Chemistry and Chemical Engineering, Xiamen University, Xiamen 361005, People's Republic of China

E-mail: jianghua.feng@xmu.edu.cn and chenz@xmu.edu.cn

Received 17 May 2013, in final form 22 August 2013
Published 21 October 2013
Online at stacks.iop.org/Nano/24/455102

Abstract
Recently, some types of MnO nanoparticle (Mn-NP) with favorable imaging capacity have been developed to improve the biocompatible profile of the existing Mn-based MRI contrast agent Mn-DPDP; however, the overall bio-effects and potential toxicity remain largely unknown. In this study, ^{1}H NMR-based metabolic profiling, integrated with traditional biochemical analysis and histopathological examinations, was used to investigate the absorption, distribution, metabolism, excretion and toxicity of Mn-NPs as candidates for MRI contrast agent. The metabolic responses in biofluids (plasma and urine) and tissues (liver, spleen, kidney, lung and brain) from rats could be divided into four classes following Mn-NP administration: Mn biodistribution-dependent, time-dependent, dose-dependent and complicated metabolic variations. The variations of these metabolites involved in lipid, energy, amino acid and other nutrient metabolism, which disclosed the metabolic fate and biological effects of Mn-NPs in rats. The changes of metabolic profile implied that the disturbance and impairment of biological functions induced by Mn-NP exposure were correlated with the particle size and the surface chemistry of nanoparticles. Integration of metabonomic technology with traditional methods provides a promising tool to understand the toxicological behavior of biomedical nanomaterials and will result in informed decision-making during drug development.

S Online supplementary data available from stacks.iop.org/Nano/24/455102/mmedia

(Some figures may appear in colour only in the online journal)

1. Introduction

Manganese (Mn) is one of the more abundant elements in the biosphere. The unique electronic configuration of the $3d^5$ shell of Mn^{2+} makes it an excellent magnetic probe for applications in the biomedical field such as drug delivery and biomedical imaging as an MRI contrast agent [1, 2]. At present, there is one commercial Mn-based MRI contrast agent, mangafodipir trisodium (Mn-DPDP), in clinical use. However, Mn-based complexes are easy to dissociate after administration to yield free Mn^{2+} because of the conversion between the six- and seven-coordinated states, which accounts for the *in vivo* instability of the Mn-DPDP chelate compared with gadolinium-based contrast agents [3]. Due to its physiological role, exposure to excess Mn can induce deleterious effects on the central nervous system and cause parkinsonism-like

syndrome, especially in patients with liver failure [4]. The *in vivo* instability of Mn-DPDP has raised especial concerns about its potential toxicity from the Mn^{2+} ions, which led to its gradual withdrawing from the market. It also suggests that it is necessary to find biocompatible and thermodynamic stable Mn compounds.

With the tremendous advances in nanotechnology, some types of Mn-NPs-based MRI contrast agent with well defined morphology and high solubility have been developed [5–7]. They exhibit favorable behaviors in detection, localization, characterization and evaluation of hepatic lesions and provide clinical advantages over the existing Mn-based MRI contrast agent, Mn-DPDP. Some of them have offered an improved biocompatible profile; however, the overall and systematic research on Mn-based nano-contrast agents is still at a relatively early stage.

Nowadays, the strategy of utilizing ADME/Tox tools for lead optimization and clinical candidate selection is the cornerstone of modern drug discovery. The traditional *in vivo* ADME/Tox studies that rely on the use of radiotracer may be still invaluable for drug standardization and assessment; however, the advances in 'omic' technologies present their challenges and advantages in drug development [8]. Metabonomics, as one of the omics, is a systematic approach for studying the dynamic metabolic response of a living system to pathophysiological stimuli, which highlights the biological variations at metabolite level and more closely mirrors the phenotype of the living system by stoichiometric analysis [9]. Thus, investigation of *in vivo* metabolic changes induced by nanoparticles may provide a detailed description of the corresponding bio-responses; further, it would help to disclose the structure–activity relationship and to elucidate the fate of nanoparticles, i.e. their distribution, degradation, metabolism and excretion [10].

In this study, we integrated ^{1}H NMR-based metabonomic strategy with the conventional biochemical methods, including blood biochemical analysis, ICP-AES determination of Mn concentration in tissues and histopathological examination, to evaluate the acute bio-related response in rats to an intravenous injection of Mn-NPs and investigate their biodistribution and metabolic fate.

2. Materials and methods

2.1. Synthesis and characterization of MnO nanoparticles

Size-homogeneous and monodisperse 10 nm MnO nanoparticles were synthesized by high-temperature thermal decomposition of manganese oleate complex as reported in the previous literature [11]. Mn-NPs dried on copper grids were visualized by transmission electron microscopy (TEM) (see figure S1 in the supplementary material available at stacks.iop.org/Nano/24/455102/mmedia). Mn-NPs were freshly well dispersed by ultrasound in saline solution before use. Prior to animal experiments, the Mn concentration of the nanoparticles in phosphate buffer solution was determined by inductively coupled plasma–atomic emission spectrometry (ICP-AES).

2.2. Animal handling and sample collection

All animal experimental protocols complied with the local guidelines for animal use and care, and all animal studies were performed at specific pathogen free (SPF) facility of Xiamen University Laboratory Animal Center (XMULAC). A total of 43 nine-week-old male SD rats (243 ± 13 g) were used in our study. The environment conditions were set at 21–26 °C with a relative humidity of 50 ± 10%, and a 12/12 h light/dark cycle. Food and tap water were provided *ad libitum*, and body weights were recorded daily. After one week of acclimatization, a single dose of Mn-NPs in saline was administrated intravenously to the rats at two dose levels of 10 mg Mn per kg body weight (bw) ($n = 15$) and 40 mg Mn per kg bw ($n = 15$). A control group ($n = 13$) was treated with saline only. Individual urine samples were collected in ice-cooled vessels containing 1% sodium azide (0.1 ml) for 2 h using a metabolic cage at time points 0, 6, 24 and 48 h post-dose (pd), respectively, and immediately frozen at −80 °C. Animals were sacrificed by exsanguination under isoflurane anesthesia at time points 6 (six rats in each group) and 48 h (remaining rats) pd. The blood sample was divided into two aliquots, one serum for biochemical analysis and the other heparinized plasma for NMR spectroscopic analysis. After weighing, brain, kidney, liver, lung and spleen tissue were excised in triplicate: one being fixed in 10% formalin for histopathological examination, the other two immediately snap-frozen in liquid nitrogen for tissue extraction and for ICP-AES analysis. These samples were stored at −80 °C until used.

2.3. Histopathology

The randomly selected samples of kidney, liver, lung and spleen tissue from Mn-NP-treated and control rats were fixed in 10% formalin. After dehydrating, the biopsies embedded in wax were sectioned at 5 μm, and stained with hematoxylin and eosin for histopathological examination by light microscopy.

2.4. Blood biochemical analysis

Clinical chemistry analysis of serum was carried out by standard spectrophotometric methods on a Roche Modular P800 automatic analyzer (Roche Diagnostics, Germany). The biochemical parameters included glucose, indirect bilirubin, total bile acid, UA, BUN, creatinine (Cn), BUN/Cn ratio, enzymes (ALT, AST, GGT, ALP, LDH and AST/ALT ratio), protein metabolism (total protein, albumin, globulin and Alb/Glo ratio) and lipid metabolism (TG, total cholesterol, HDL-C and LDL-C). All parameters are expressed as mean ± standard deviation (SD).

2.5. Sample preparation and ^{1}H NMR spectroscopic analysis

Samples of plasma (255 μl) were mixed with 255 μl of deuterated phosphate buffer solution (NaH_2PO_4 and K_2HPO_4, 60 mM, pH 7.4). After centrifugation at 10 000 *g*

at 4 °C for 10 min to remove the precipitates, 500 μl of the supernatants was transferred into a 5 mm NMR tube and analyzed by NMR spectroscopy. ^{1}H NMR spectra of these samples were acquired using a 500 MHz Varian spectrometer at 296 K. Standard 1D ^{1}H spectra were acquired with a water-suppressed CPMG pulse sequence. For each sample, 64 FIDs were collected into 20 K data points over a spectral width of 10 000 Hz with a relaxation delay of 0.23 ms.

Samples of urine (455 μl) were mixed with 55 μl of deuterated phosphate buffer solution (NaH_2PO_4 and K_2HPO_4, 1.5 M, including 0.1% TSP (sodium 3-(trimethylsilyl) propionate-2,2,3,3-d_4), pH 7.4) to minimize any gross variation in the pH of the urine samples. The mixture was left to stand for 10 min and centrifuged at 10 000 *g* at 4 °C for 10 min to remove the precipitates. 500 μl of the supernatants were transferred into a 5 mm NMR tube and analyzed by NMR spectroscopy. ^{1}H NMR spectra of these samples were acquired using the standard NOESYPR1D pulse sequence on a 500 MHz Varian spectrometer at 296 K. For each sample, 128 FIDs were collected into 40 K data points over a spectral width of 10 000 Hz with a relaxation delay of 0.23 ms.

The polar metabolites in the rat tissue were extracted according to the protocol established by Wu *et al* [12]. In brief, pre-weighed brain, kidney, liver, lung, or spleen samples (100 mg per sample) were homogenized in 400 μl of CH_3OH and 85 μl of H_2O at 4 °C. The homogenates were transferred into a 2.5 ml tube, and combined with 400 μl of $CHCl_3$ and 200 μl of H_2O and then kept in vortex for 60 s. After 10 min partitioning on ice, the samples were centrifuged for 5 min (10 000 *g*, 4 °C). The upper supernatants were transferred into 1.5 ml tubes, and lyophilized to remove CH_3OH and H_2O. The extracts were reconstituted in 0.5 ml D_2O containing 1 mM TSP, then transferred into 5 mm NMR tubes and analyzed by NMR spectroscopy. ^{1}H NMR spectra of these samples were acquired on a Bruker-AV600 spectrometer at 296 K. Standard 1D ^{1}H spectra were acquired with a 'ZGPR' pulse sequence. For each sample, 64 free induction decays (FIDs) were collected into 64 k data points over a spectral width of 12 000 Hz with a relaxation delay of 6.5 μs and an acquisition time of 2.66 s.

2.6. Spectral processing and pattern recognition

The FIDs were multiplied by an exponential function corresponding to a 1 Hz line-broadening factor before Fourier transformation. The acquired NMR spectra were manually phased and baseline-corrected using Bruker TOPSPIN 3.0 and referenced to the CH_3 resonance of lactate at δ 1.33 for plasma spectra and TSP at δ 0.00 for urine and tissue extract samples. The peaks observed were assigned on the basis of their chemical shifts and signal multiplicity [13].

Each ^{1}H NMR spectrum of plasma, urine, or aqueous tissue extract was segmented into regions of 0.005 ppm using AMIX (v.3.8, Bruker Biospin). The segments of δ 6.0–5.5 and δ 5.20–4.29 in the plasma spectra (δ 9.0–0.5), and of δ 6.02–5.45 and δ 5.35–4.24 in the urine spectra (δ 9.5–0.5) were removed to exclude the urea signal and the uncertainty of residual water signal. In the case of the chloroform/methanol tissue extract, the regions of δ 5.226–4.675 and δ 3.40–3.31 in the spectra were excluded to remove variation in residual water and methanol signal.

Normalization was applied to the total sum of integrated data from each sample, which makes the data directly comparable with each other. The mean centered data were analyzed by principal component analysis (PCA) to reveal trends, highlight outliers, and show clusters among the observations in SIMCA-P+ 11.0 (Umetrics, Sweden). Then, the orthogonal projection to latent structure with discriminant analysis (OPLS-DA) method was utilized to identify the differential metabolites responsible for Mn-NP exposure on unit variance scaled data. Score plots provide the most efficient 2D representation of the information contained in the data set, and the corresponding coefficient loading plots were used to describe the influence of the variables on the scores. Here, a correlation coefficient (determined by the Pearson's product-moment correlation coefficient) of $|r| > 0.755$ (the degree of freedom is equal to 5) was used as the cut-off value that gave a statistically significant result at the level $P < 0.05$.

2.7. Statistical analysis

The data were expressed as mean ± SD. Inter-group variations were assessed by one-way analysis of variance (ANOVA) followed by a post hoc Fisher least significant difference test. The criterion for statistical significance was $p < 0.05$.

3. Results and discussion

3.1. Effect of Mn-NPs on gross histological morphology

Microscopic examinations were conducted on the selected tissues from low-dose (10 mg Mn kg^{-1}), high-dose (40 mg Mn kg^{-1}), and control rats. No apparent pathological change was observed in the kidney after administration compared with the controls (figure S2 in the supplementary material available at stacks.iop.org/Nano/24/455102/mmedia). The portal area of the liver and hepatocytes around the central vein showed normal results, except a moderate increase in the white blood cell count displayed around the bile ducts at 48 h after high-dose Mn-NP administration (denoted by an arrow in figure 1(B)). No obvious histological change in the lung was observed in any treatment group compared with the controls, although there was a relative lymphocytosis in the lung interstitium of the high-dose group at 48 h after treatment (figure 1(D)). No apparent histological change was observed in the spleen in either the low- or high-dose group at 6 h after administration (data not shown); however, at 48 h after administration the spleen was characterized as a mild enlarged area of white pulp with red pulp normal (denoted by arrow in figure 1(F)).

3.2. The ratios of tissue to body weights

Figure 2 shows the ratios of the tissues to body wet-weight. The only change in the L48 group came from the ratio

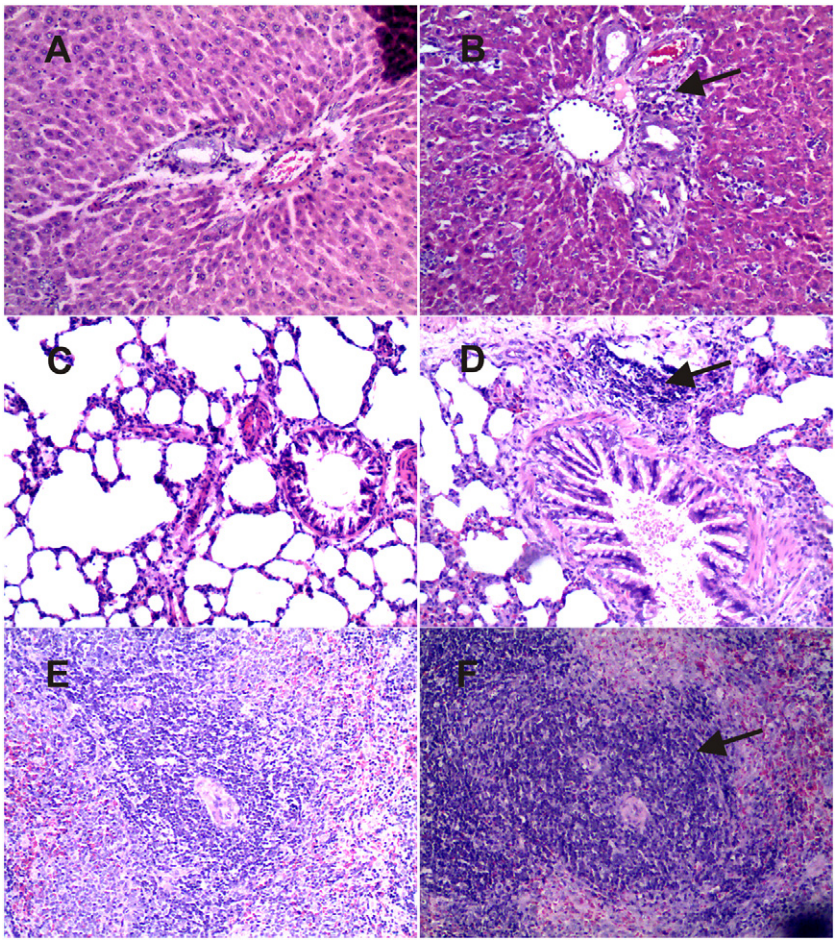

Figure 1. Photomicrographs of representative sections of the liver ((A) and (B)), lung ((C) and (D)), and spleen ((E) and (F)) from control ((A), (C) and (E)) and high-dose ((B), (D) and (F)) Mn-NP-treated rats at 48 h pd. The tissue sections were stained with hematoxylin–eosin and observed under a 100× microscope. The arrows in (B) and (D) show the increased inflammatory cells in the liver and the lung, respectively, and the arrow in (F) shows the mild enlarged area of white pulp in the spleen.

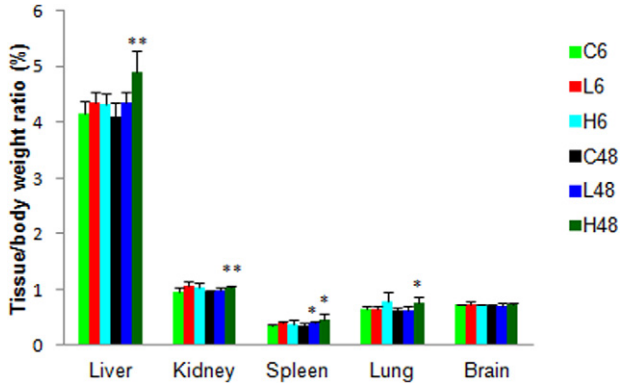

Figure 2. Effect of MnO nanoparticle administration on tissue/body weight ratio (%). C, control group; L, low-dose group; H, high-dose group; 6, 6 h post-dose; 48, 48 h post-dose.
* Significant differences between two groups as judged by Student's *t*-test (*$P < 0.05$; **$P < 0.001$).

of spleen/BD, which increased to 114% of control ($P < 0.05$), while the ratios of kidney/BD, liver/BD, lung/BD, and spleen/BD in the H48 group showed increases to 108% ($P < 0.001$), 119% ($P < 0.001$), 122% ($P < 0.05$), and 131% ($P < 0.05$) of control, respectively. We assume that both Mn-NP-induced body weight loss and tissue weight gain due to inflammation contributed to this rise of the ratios, as observed in microscopic examination (figure 1).

3.3. Biodistribution of Mn in the different tissues

The distribution of Mn-NPs in tissues was evaluated by ICP-AES (figure 3). Most of the nanoparticles were transferred into liver and spleen following the low-dose Mn-NP administration. By contrast, high-dose Mn-NPs induced a more widespread tissue distribution. Mn-NP contents in liver, lung, and spleen demonstrated a similar deposited order: H6 > L6 > H48 > L48 within their respective groups; however, a different deposited order, H6 > H48 > L6 > L48, was displayed in the brain and kidney. These results demonstrate a varied biodistribution and excretion in the different tissues. Furthermore, according to the data, the overall clearance rate of Mn-NPs from lung and spleen was faster than that from kidney and liver, while it was the slowest to clearance from the brain. Such observation

Table 1. Effect of MnO nanoparticle administration on blood biochemical indices.

Indices	C6[a]	L6	H6	C48	L48	H48
TP (g/L)[b]	43.65 ±7.36[c]	54.10 ± 2.10[d]	47.33 ± 3.37	56.63 ± 2.88	58.47 ± 2.36	54.58 ± 3.21
Alb (g/L)	25.20 ± 3.43	30.08 ± 0.62[d]	27.47 ± 1.38	31.36 ± 0.95	29.04 ± 0.68[e]	26.76 ± 1.54[e]
Glo (g/L)	18.45 ± 4.15	24.02 ± 1.61[d]	19.87 ± 2.10	25.27 ± 1.97	29.42 ± 1.77[e]	27.82 ± 1.98[d]
Alb/Glo	1.39 ± 0.17	1.26 ± 0.07	1.39 ± 0.10	1.25 ± 0.06	0.99 ± 0.04[e]	0.96 ± 0.05[e]
Ibil (μmol/L)	1.00 ± 0.39	1.47 ± 0.14[d]	1.62 ± 0.23[d]	1.66 ± 0.20	1.48 ± 0.10[d]	1.72 ± 0.23
ALT (U/L)	34.40 ± 8.44	64.67 ± 8.16[e]	122.40 ± 27.68[e]	42.50 ± 2.07	50.22 ± 6.85[d]	43.33 ± 7.31
AST (U/L)	145.20 ± 38.15	265.50 ± 18.36[e]	623.17 ± 107.85[e]	178.00 ± 18.69	164.33 ± 28.43	137.22 ± 25.60[e]
AST/ALT	3.57 ± 1.06	4.15 ± 0.46	4.65 ± 0.98	4.07 ± 0.49	3.31 ± 0.69[d]	3.20 ± 0.53[d]
GGT (U/L)	0.08 ± 0.04	2.00 ± 0.00[e]	3.67 ± 1.75[d]	0.10 ± 0.00	0.80 ± 0.40[e]	4.38 ± 2.33[e]
ALP (U/L)	211.20 ± 37.93	321.67 ± 38.54[e]	295.83 ± 26.70[d]	309.00 ± 58.58	322.89 ± 74.70	363.38 ± 52.37
TG (mmol/L)	0.76 ± 0.16	1.84 ± 0.37[e]	1.99 ± 0.73[d]	0.99 ± 0.27	0.59 ± 0.11[d]	0.82 ± 0.29
TC (mmol/L)	1.86 ± 0.34	2.57 ± 0.35[e]	2.32 ± 0.19[d]	2.32 ± 0.14	2.74 ± 0.20[e]	3.00 ± 0.34[e]
HDL-C (mmol/L)	0.51 ± 0.09	0.71 ± 0.06[e]	0.58 ± 0.05	0.68 ± 0.07	0.81 ± 0.06[e]	0.71 ± 0.14
LDL-C (mmol/L)	0.15 ± 0.05	0.29 ± 0.11[d]	0.21 ± 0.04[d]	0.19 ± 0.02	0.37 ± 0.08[e]	0.57 ± 0.09[e]
Glc (mmol/L)	4.93 ± 0.58	5.98 ± 0.88[d]	3.94 ± 0.56[d]	4.37 ± 0.35	3.96 ± 0.88	3.63 ± 0.83[d]
LDH (U/L)	1241.62 ± 244.45	791.42 ± 189.04[d]	1468.97 ± 67.72	1464.27 ± 80.92	1210.10 ± 181.58[d]	526.71 ± 79.73[e]
BUN (mmol/L)	3.82 ± 1.56	6.26 ± 0.88[d]	14.09 ± 3.67[e]	5.80 ± 1.08	5.05 ± 0.68	4.62 ± 1.01[d]
Cn (μmol/L)	34.20 ± 3.56	47.00 ± 3.35[e]	54.67 ± 10.46[d]	57.14 ± 3.63	54.44 ± 2.74	50.11 ± 1.62[e]
BUN/Cn	0.10 ± 0.02	0.13 ± 0.01[e]	0.26 ± 0.04[e]	0.10 ± 0.01	0.09 ± 0.01	0.09 ± 0.02
UA (μmol/L)	141.00 ± 58.89	165.33 ± 43.89	143.83 ± 15.65	135.43 ± 34.67	172.00 ± 39.96	186.00 ± 38.81[d]
TBA (μmol/L)	33.60 ± 19.64	21.00 ± 8.19	22.42 ± 4.41	34.67 ± 14.30	21.94 ± 10.53	18.98 ± 5.38[d]

[a] C, control group; L, low-dose group; H, high-dose group; 6, 6 h post-dose; 48, 48 h post-dose.

[b] TP, total protein; Alb, albumin; Glo, globulin; Ibil, indirect bilirubin; ALT, alanine aminotransferase; AST, aspartate aminotransferase; GGT, gamma glutamyltransferase; ALP, alkaline phosphatase; TG, triglycerides; TC, total cholesterol; HDL, high-density lipoprotein, LDL, low-density lipoprotein; Glc, glucose; LDH, lactate dehydrogenase; BUN, blood urea nitrogen; Cn, creatinine; UA, uric acid; TBA, total bile acid.

[c] Each data value represents the mean ± SD.

[d] Significant differences between two groups as judged by Student's *t*-test using SPSS with $P < 0.05$.

[e] Significant differences between two groups as judged by Student's *t*-test using SPSS with $P < 0.001$.

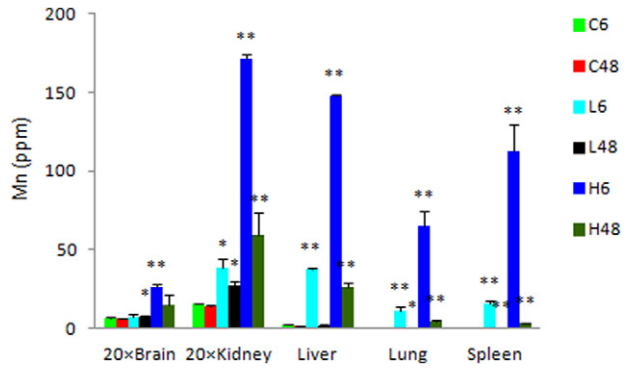

Figure 3. Effect of MnO nanoparticle administration on biodistribution of Mn. C, control group; L, low-dose group; H, high-dose group; 6, 6 h post-dose; 48, 48 h post-dose; 20×, multiplied 20-fold. * Significant differences between two groups as judged by Student's *t*-test (*$P < 0.05$; **$P < 0.001$).

together with the histological results suggests that liver, not kidney, was the main organ for disposal and clearance of Mn-NPs from the circulation.

3.4. Effect of Mn-NPs on serum biochemical parameters

Hepatocytes are responsible for synthesis of most of the serum proteins, so serum proteins, including total protein (TP), albumin (Alb), globulin (Glo), and albumin to globulin ratio (Alb/Glo), were determined to evaluate liver function. Table 1 shows a mild increase in TP, Alb, and Glo levels in the low-dose group at 6 h pd. However, a slight reduction of Alb and a mild rise of Glo resulted in a significant decrease ($P < 0.001$) in Alb/Glo ratio in both low- and high-dose groups at 48 h pd (table 1). It is probable that Mn-NPs bound to carrier proteins such as Alb, Glo, or even apolipoprotein and induced upregulation of these carrier proteins as a protective response [14].

γ-glutamyl transpeptidase (GGT), primarily present in microsomal membranes of biliary epithelium, plays a key role in glutathione (GSH) metabolism and xenobiotic detoxification. Elevated serum GGT activity commonly indicates bile duct or liver disease. Another sensitive biochemical marker is alkaline phosphatase (ALP) to detect obstructive biliary disease. Table 1 shows that GGT activities in low- and high-dose groups were sharply increased by 25.0- and 45.9-fold at 6 h pd and 8.0- and 43.8-fold at 48 h pd, respectively, while ALP elevations were moderate, to 152% ($P < 0.001$, low-dose group) and 140% ($P < 0.05$, high-dose group) at 6 h pd, and returned nearly to control level 48 h pd (table 1). It is reasonable to assume that Mn-NP-induced hepatocellular jaundice led to moderate elevation in ALP activity and partially contributed to the

elevation of GGT activity in serum, and Mn-NP-induced oxidative stress possibly further increased the activity of GGT.

The activities of ALT and AST increased to 188% ($P < 0.001$) and 183% ($P < 0.001$) in the low-dose group and to 356% ($P < 0.001$) and 429% ($P < 0.001$) in the high-dose group 6 h pd, respectively, and both enzyme activities recovered nearly to the normal level at 48 h pd. The ratios of AST/ALT in both the low- and high-dose groups show significant decrease ($P < 0.05$) at 48 h pd. Clinically, the change of their ratio can serve as an indication of liver injury, in which a decrease implies mild hepatic injury and an increase implies severe hepatic injury. Our results suggest that the Mn-NP exposure had a slight effect on the normal liver function at 48 h pd.

The concentrations of total cholesterol (TC) and HDL-C in both Mn-NP-treated groups were increased at both 6 h and 48 h pd (table 1). Similarly, the levels of LDL-C were severely elevated. The triglyceride (TG) level moderately increased at 6 h pd, but mildly decreased at 48 h pd (table 1). In addition, the mean level of total bile acid (TBA) in all Mn-NP-treated groups was decreased moderately, while only in the high-dose group it was statistically significant at 48 h pd. The liver plays a central role in cholesterol metabolism. Cholesterol, from the diet or from *de novo* synthesis, is not only secreted by hepatocytes for exporting to other cells, but also converted to bile acids via cytochrome P450-mediated oxidation and secreted into the intestine. The *in vitro* studies have shown that substitution of heme iron with Mn inhibits the enzyme activity of cytochrome P450 [15]. Therefore, we assume that Mn ion release of Mn-NPs substituted the heme iron of cytochrome P450 and reduced the efficiency of bile synthesis and secretion. Furthermore, it has been confirmed that the elevation of bilirubin level (table 1) and excess Mn ions induced intrahepatic cholestasis, which caused further reduction of bile salt secretion [16]. The inability of liver to convert cholesterol from LDL and HDL into bile salts led to the increased level of TC, HDL-C and LDL-C in serum. The decrease of bile secretion affected the ensuing digestion and absorption of fats and bile salts in the small intestine, which directly led to the significant decrease of TG and TBA levels at 48 h pd (table 1).

As shown in table 1, exposure of rats to Mn-NPs resulted in an increase of creatinine (Cn) to 137% ($P < 0.001$) and 160% ($P < 0.05$), and the blood urea nitrogen (BUN) level was severely increased to 164% ($P < 0.05$) and 369% ($P < 0.001$), while the corresponding ratio of BUN/Cn rose to 130% ($P < 0.001$) and 260% ($P < 0.001$) of control in low- and high-dose groups at 6 h pd, respectively. At 48 h pd, no apparent change was measured in the levels of Cn, BUN and uric acid (UA) and the ratio of BUN/Cn between the low-dose group and the control, while the results of the high-dose group showed a decreased level of Cn (88%, $P < 0.001$) and BUN (80%, $P < 0.05$), and an increased level of UA (137%, $P < 0.001$). Cn is generated in muscle with a fairly constant rate, and is filtered out of the blood by the kidney. The histological results showed no obvious change in renal structure upon Mn-NP treatment. Therefore, we think that, beyond glomerular filtration capacity, both hemolysis of red blood induced by Mn-NPs and electrolyte disturbance/imbalance caused by the ion release of Mn-NPs contributed to the elevation of Cn, BUN, and the ratio of BUN/Cn at 6 h pd, while the concurrent actions from hemolytic anemia and hypohepatia caused the decreased levels of Cn and BUN in the high-dose group at 48 h pd.

3.5. ^{1}H *NMR profiles of biological fluids and tissues from rats*

Representative ^{1}H NMR spectra of biological fluids (plasma and urine) and tissue extracts (brain, lung, kidney, spleen and liver) are shown in figure 4. The primary peaks in the spectra were assigned to individual metabolites (table S1 in the supplementary materials available at stacks.iop.org/Nano/24/455102/mmedia) according to previous studies [13, 17], and confirmed by a public NMR database (Human Metabolome Database V3.0, see www.hmdb.ca) and an in-house developed NMR database.

To get the overall metabolic information and examine the intrinsic variation within the respective biocompartment, unsupervised PCA was performed on the respective NMR data sets. In the representative score plots (shown in figure 5), the value of R^2X in the lower left corner of plots represents the explainable variance and the value of Q^2 in the lower right corner of plots is a measure of the predictive power of the model in each panel. PCA results reveal that the clusters of plasma and the extracts of kidney, liver, and spleen from Mn-NP-treated groups were distinct from those of the corresponding controls, which implies an obvious change in the metabolic profiles induced by Mn-NPs, while the samples of urine and the extracts of brain and lung display some degree of overlap between the controls and the corresponding dosed groups, which suggests a moderate effect induced by Mn-NPs on these biological compartments. Additionally, urinary metabonomic recovery in the high-dose group could be observed to a certain degree, though not complete, which offers some clues to the biochemical processing of Mn-NPs in the body. The supervised OPLS-DA model was then used to identify the metabolic difference between the groups. The OPLS-DA score plots (left panels in figures 6 and S3 available at stacks.iop.org/Nano/24/455102/mmedia) give a clear separation between Mn-NP-treated groups and the corresponding controls, and the OPLS-DA loading plots (middle and right panels in figures 6 and S3 available at stacks.iop.org/Nano/24/455102/mmedia) offer an insight into the types of metabolite responsible for the separation, based on the first principal component. The significant class-discriminating metabolites corresponding to all pairwise groups are tabulated in tables 2, 3(A) and (B), and S2 (available at stacks.iop.org/Nano/24/455102/mmedia), and provide the biochemical alterations in the different biocompartments following the administration of Mn-NPs.

3.5.1. Metabonomic analysis of plasma. According to OPLS-DA analysis of NMR data from plasma (table 2), the levels of 1-methylhistidine, VLDL, $-CH_2-CH_2-C{=}O$ (L5), allantoin, leucine (Leu), threonine (Thr), glycerophosphocholine (GPC), pyruvate, glutamine (Gln), choline,

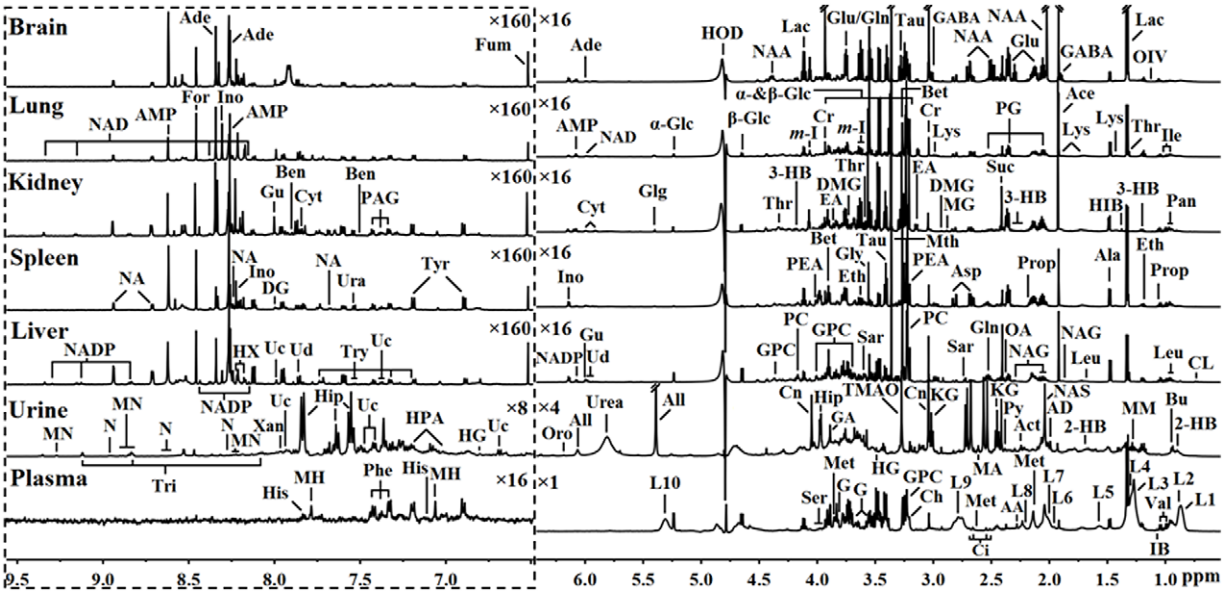

Figure 4. Typical ^{1}H NMR spectra of plasma, urine and aqueous brain, lung, kidney, spleen and liver extracts from a low-dosed rat at 6 h pd. The region of δ 6.5–9.5 (in the dashed box) in the spectrum was magnified 16-, two- or tenfold in vertical expansion compared with the corresponding region of δ 0.5–6.4. AA, acetoacetate; Ace, acetate; Act, acetone; AD, acetamide; Ade, adenosine; AH, aminohippurate; Ala, alanine; All, allantoin; AMP, adenosine monophosphate; Asp, aspartate; Ben, benzoate; Bet, betaine; Bu, butyrate; Ch, choline; Ci, citrate; CL, cholate; Cn, creatinine; Cr, creatine; Cyt, cytidine; DG, deoxyguanosine; DMA, dimethylamine; DMG, *N*,*N*-dimethylglycine; EA, ethanolamine; Eth, ethanol; For, formate; Fum, fumarate; G, glycerol; GA, guanidinoacetate; GABA, gamma-aminobutyrate; Glg, glycogen; α-Glc, alpha-glucose; β-Glc, beta-glucose; Gln, glutamine; Glu, glutamate; Gly, glycine; GPC, glycerophosphocholine; GSH, glutathione; Gu, guanosine; 2-HB, 2-hydroxybutyrate; 3-HB, 3-hydroxybutyrate; HG, homogentisate; HIB, 2-hydroxyisobutyrate; Hip, hippurate; His, histidine; *p*-HPA, para-hydroxyphenylacetate; HX, hypoxanthine; m-I, *myo*-inositol; IB, isobutyrate; Ile, isoleucine; Ino, inosine; KG, alpha-ketoglutarate; L1, LDL, $\underline{C}H_3$ –$(CH_2)_n$–; L2, VLDL, $\underline{C}H_3$ –$(CH_2)_n$–; L3, LDL, CH_3– $(C\underline{H}_2)_n$–; L4, VLDL, CH_3– $(C\underline{H}_2)_n$–; L5, VLDL, –$C\underline{H}_2$ –CH_2–C=O; L6, lipid, –$C\underline{H}_2$ –CH=CH–; L7, lipid, –$C\underline{H}_2$ –CH_2–CH=CH–; L8, lipid, –CH_2–C=O; L9, lipid =CH–CH_2–CH=; L10, lipid, –CH=CH–; Lac, lactate; Leu, leucine; Lys, lysine; MA, methylamine; Met, methionine; MG, methylguanidine; MH, 1-methylhistidine; 3-MH, 3-methylhistidine; MM, methylmalonate; MN, 1-methylnicotinamide; Mol, methanol; N, nicotinate; NA, nicotinamide; NAA, *N*-acetylaspartate; NAD, NAD^+; NADP, $NADP^+$; NAG, *N*-acetylglutamate; NAS, *N*-acetylglycoprotein signals; OA, oxaloacetate; OAS, *O*-acetylglycoprotein signals; OIV, 2-oxoisovalerate; Oro, orotate; PAG, phenylacetylglycine; Pan, pantothenate; PC, phosphocholine; PEA, phosphoethanolamine; PG, pyroglutamate; Phe, phenylalanine; Prop, propionate; Py, pyruvate; Sar, sarcosine; Ser, serine; Suc, succinate; Tau, taurine; Thr, threonine; TMAO, trimethylamine *N*-oxide; tri, trigonelline; Trp, tryptophan; Tyr, tyrosine; Uc, urocanate; Ud, uridine; U-Glc, uridine diphosphate glucose; Ura, uracil; Val, valine; Xan, xanthine.

citrate, and phenylalanine (Phe) were changed only in the high-dose group at 6 h pd, while lipid –CH_2–C=O (L8), tyrosine (Tyr), and lactate were changed in all groups except the low-dose group at 48 h pd. In contrast, the levels of isobutyrate, LDL CH_3–$(CH_2)_n$–(L1), VLDL CH_3–$(CH_2)_n$–(L2), LDL CH_3–$(CH_2)_n$–(L3), lipid –CH_2–CH=CH–(L7), lipid –CH=CH– (L10), alanine (Ala), methionine (Met), lysine (Lys), glycerol, *myo*-inositol, lipid –CH_2–CH_2–CH=CH– (L6), *O*-acetylglycoprotein, serine (Ser), creatine, glycine (Gly), formate, and isoleucine (Ile) exhibited a time-dependent response. However, the levels of *N*-acetylglycoprotein, betaine, lipid =CH–CH_2–CH= (L9), acetone, acetate, and glucose were changed in a complicated manner.

Consistent with blood biochemical analysis (table 1), the elevated lipid levels in the plasma samples at 6 h pd were followed by a drop. We hypothesize that Mn-NP exposure depleted the main substrates of oxidative phosphorylation, namely oxygen and glucose, during the period of acute response, and induced a metabolic switch from glucose to fatty acid oxidation, which stimulated lipolysis and fatty acid release into the bloodstream, and finally resulted in a rise of fatty acids, triglycerides, lipoproteins, and ketone bodies such as acetone (figure 6 and table 2).

Choline, sarcosine, dimethylamine, Met, formate, and betaine are the sources of methyl groups. The methylation process helps the body to respond to stress, to detoxify xenobiotics, and to create new cells. Methyl deficiency, as reflected in low levels of those metabolites with methyl sources such as choline, Met, formate, and betaine at different time points (table 2), suggests that methylation played an important role in the detoxification of Mn-NP exposure. Similar results were also observed in the corresponding splenic, hepatic, and urinary metabonomes (tables 3(A) and (B)).

1-methylhistidine is derived from anserine via the hydrolysis of carnosinase. Previous studies showed that Mn^{2+} ions increased the activity of carnosinase [18]. The increased level of 1-methylhistidine (table 2) may be a natural outcome of the activated carnosinase. Besides, its elevation may also be a stimulating action to hemopoietic function for compensating the decrease in the number of erythrocytes from the hemolysis

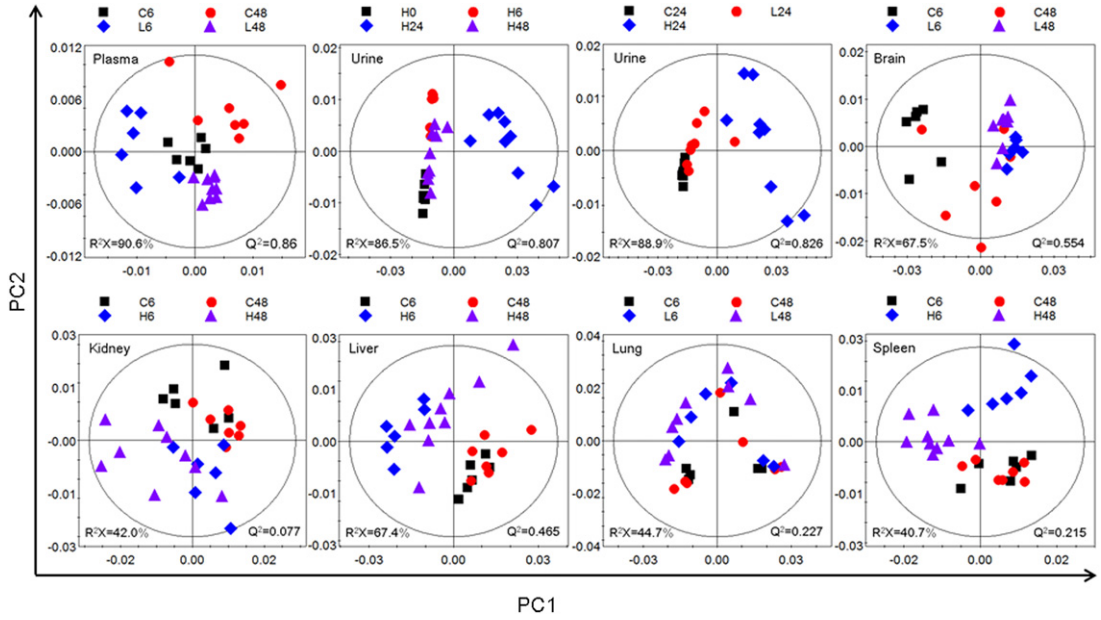

Figure 5. Representative PCA score plots (PC1 versus PC2) derived from the ^{1}H NMR data of body fluid samples (plasma and urine) and tissue samples (extracted from brain, kidney, liver, lung, and spleen) from the corresponding groups of rats: C, control group; L, low-dose group; H, high-dose group; 0, 0 h post-dose; 6, 6 h post-dose; 24, 24 h post-dose; 48, 48 h post-dose.

induced by nanoparticle exposure. In addition, allantoin is the end-product of purine metabolism in rats. The reduction of allantoin in the brain and liver and the increase in blood and urine (figure 6, table 2) suggest that Mn-NPs promoted both the secretion of allantoin from tissues and the excretion through the kidneys.

3.5.2. Metabonomic analysis of urine. The body's metabolites are exchanged between blood and organs and then transported into the kidneys, where metabolic wastes are finally excreted into the urine. Thus urine formation is a time-consuming process. Analysis of the urinary metabolites (figure 6, table 2) may provide the time- and dose-response information that can be used to determine the onset and severity of toxicity [9]. The changes in metabolite concentrations at 6 h pd seemed to be linked to the early effects of Mn-NPs on the kidney and circulatory system, displayed in the concentration variations of *N*-phenylacetylglycine, citrate, allantoin, methylmalonate, creatine, formate, xanthine, acetamide, 1-methylnicotinamide, acetone, 2-oxoisovalerate, and succinate, while the changes at 48 h pd could reflect the metabolic alterations in the other organs upon Mn-NP exposure, which included the concentration variations of nicotinate, lactate, hippurate, betaine, 4-hydroxyphenylacetate, methylamine, Ala, and Gly. The alterations in the contents of Cn, urocanate, and guanidinoacetate showed a dose-dependent response, while some other metabolites demonstrated a complicated effect of time and dose responses.

Niacin, also known as vitamin B_3, inhibits the release of free fatty acids from the adipocytes. A decrease in urinary excretion of niacin and its metabolites trigonelline and nicotinamide *N*-oxide may mean that more niacin and its metabolites were kept in the body to cope with the high serum lipid levels that have been observed in serum biochemical analysis. In addition, MNA has been proven to be an antithrombotic, which regulated thrombotic and inflammatory processes in the cardiovascular system by a mechanism involving cyclooxygenase-2 and prostacyclin [19]. The increased level of MNA in the urine suggests that high-dose Mn-NP exposure possibly caused thrombosis or inflammation in the circulatory system.

Usually, elevated Cn levels in urine are a sign of impaired kidney function, while in this case we suppose the increases of urinary creatine and Cn excretion in the high-dose group were due to the increased protein catabolism. This is consistent with the conclusion drawn from the serum biochemical analysis. Guanidinoacetate is synthesized from arginine and Gly, and consumes a methyl group to form creatine. In addition, as the product in histidine catabolism and the substrate of urocanase, the decreased level of urocanate in the high-dose group may reflect the activation of urocanase by Mn^{2+} [20].

The detoxification process for the toxic effect induced by Mn-NPs caused a vitamin B_{12} deficiency, which made it unavailable to catalyze conversion of methylmalonate into succinate, and thus led to a high methylmalonate level and a low succinate present in urine. Mn is an essential co-factor for xanthine oxidase, and Mn-NPs stimulated this enzyme, which converts xanthine to UA, and subsequently to allantoin. This may be the reason for the diminished excretion of xanthine and the elevated excretion of allantoin.

N-phenylacetylglycine (PAG) is a putative biomarker of phospholipidosis, and the elevation of urinary PAG indicated the impact of Mn-NP exposure on phospholipid metabolism. In addition, consistent with the plasma NMR data, low urinary citrate and alpha-ketoglutarate excretion suggest that Mn-NP exposure caused a switch from aerobic to anaerobic respiration and induced the alteration of Ala, ethanol, and

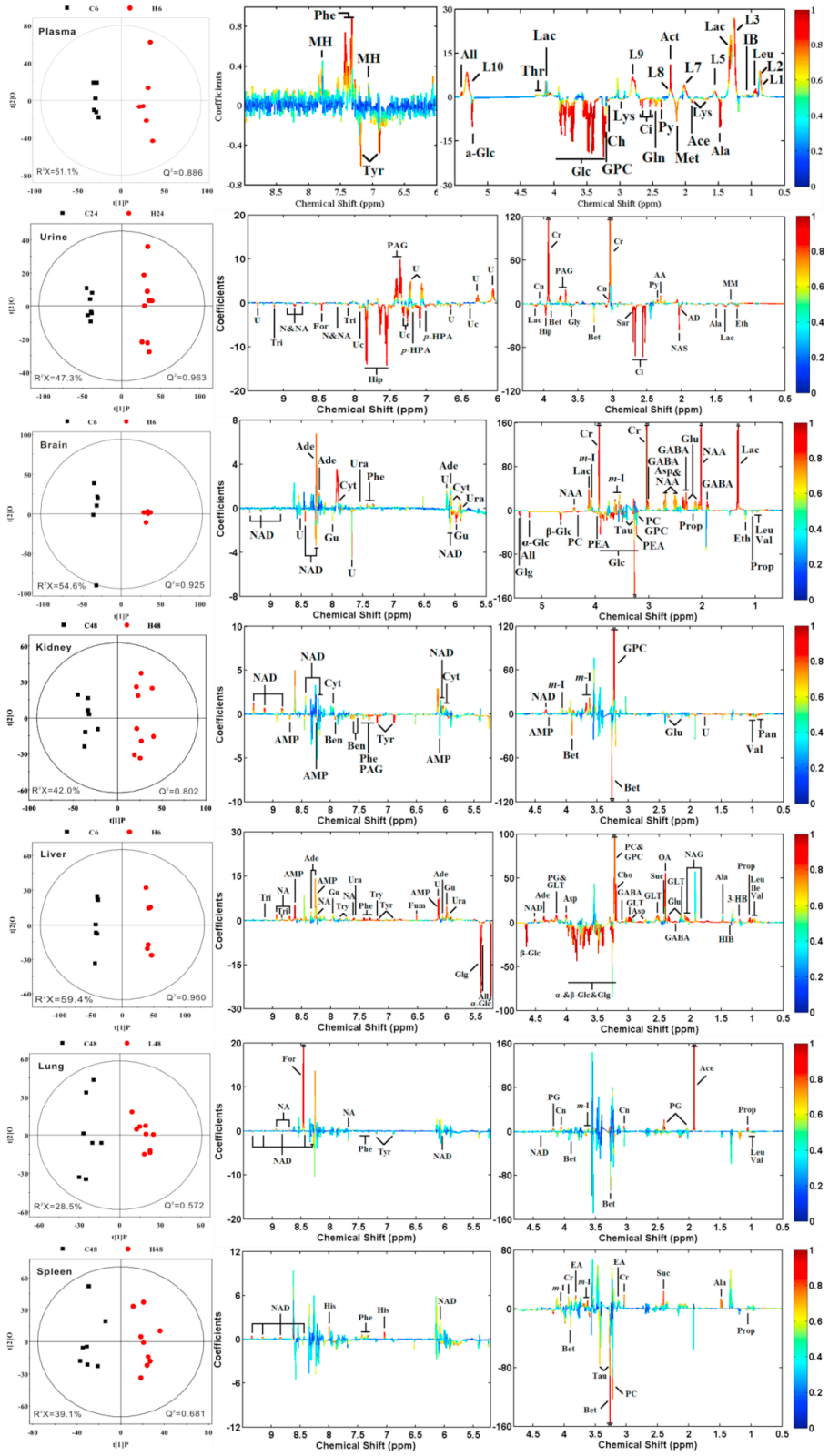

Figure 6. Representative OPLS-DA score plots (left panel) derived from the ^{1}H NMR data of body fluid samples (plasma and urine) and tissue samples (extracted from brain, kidney, liver, lung, and spleen) and corresponding coefficient loading plots (middle and right panels) obtained from different pairwise groups. C, control group; L, low-dose group; H, high-dose group; 6, 6 h post-dose; 24, 24 h post-dose; 48, 48 h post-dose. Q^2 indicates the predictability of the model, and R^2X represents the total explainable variation. The color code corresponds to the correlation coefficients of the metabolic variables. The loading plots identifying discriminatory metabolites between pairwise classes are based on the first principal component (t[1]P). Signals with a positive direction relate to the abundance of metabolites in the groups in the positive direction of t[1]P, and vice versa. Keys for the assignments are shown in the notes of figure 2 and the detailed information is listed in tables 2, 3, S2, and S3 (available at stacks.iop.org/Nano/24/455102/mmedia).

Table 2. Summary of metabolic variations in rat body fluids induced by Mn-NPs between different pairwise groups.

Plasma					Urine					
Metabolites	C6–L6	C6–H6	C48–L48	C48–H48	Metabolites	C6–L6	C6–H6	C24–L24	C24–H24	C48–L48	C48–H48
MH[a]	—	0.85	—	—	MN	—	0.76	—	—	—	—
L5	—	0.93	—	—	Act	—	0.85	—	—	—	—
All	—	0.87	—	—	OIV	—	0.89	—	—	—	—
Leu	—	0.84	—	—	Suc	—	−0.92	—	—	—	—
Thr	—	0.80	—	—	AD	—	−0.89	—	−0.88	—	—
GPC	—	−0.91	—	—	Cr	—	0.76	—	0.98	—	—
Py	—	−0.93	—	—	For	—	−0.92	—	−0.88	—	—
Gln	—	−0.78	—	—	MM	—	0.91	—	0.82	—	—
Ch	—	−0.76	—	—	Xan	—	−0.89	—	−0.79	—	—
Ci	—	−0.94	—	—	All	0.87	0.77	—	0.82	—	0.89
Phe	0.81	0.95	—	0.77	PAG	0.75	0.89	0.86	0.94	—	0.80
L8	0.79	0.93	—	0.91	Ci	−0.83	−0.95	−0.89	−0.98	—	−0.90
Tyr	−0.89	−0.88	—	−0.78	Ala	—	—	—	−0.87	—	—
Lac	−0.81	0.92	—	−0.80	Gly	—	—	—	−0.80	—	—
IB	0.94	0.77	—	—	MA	—	—	—	−0.88	—	—
L1	0.95	0.79	—	—	*p*-HPA	—	—	−0.81	−0.86	—	—
L2	0.90	0.75	—	—	Bet	—	—	−0.78	−0.75	—	−0.81
L3	0.89	0.91	—	—	Hip	—	—	−0.78	−0.93	—	−0.95
L7	0.89	0.88	—	—	Lac	—	—	−0.81	−0.88	—	−0.85
L10	0.90	0.86	—	—	N	—	—	−0.86	−0.95	−0.92	−0.91
Ala	−0.96	−0.96	—	—	Cn	—	0.77	—	0.85	—	0.81
Met	−0.76	−0.83	—	—	Uc	—	−0.76	—	−0.91	—	−0.77
Lys	−0.90	−0.86	0.75	0.78	GA	—	—	0.81	—	0.79	—
G	—	—	0.95	0.91	Ch	0.84	—	—	—	—	—
m-I	—	—	0.93	0.92	KG	−0.87	−0.98	—	—	—	—
L6	—	—	0.92	0.91	AA	—	—	0.81	0.87	—	—
OAS	—	—	0.96	0.93	2-HB	—	—	0.81	—	—	—
Ser	—	—	—	0.88	Tau	—	—	—	—	—	−0.87
Cr	—	—	—	0.79	NAS	—	−0.96	−0.84	−0.94	—	−0.88
Gly	—	—	—	0.85	Tri	—	−0.96	−0.87	−0.97	—	−0.82
For	—	—	—	−0.78	Eth	—	0.83	—	−0.92	—	—
Ile	—	—	−0.80	—	Py	—	−0.88	0.79	0.80	—	0.83
NAS	0.88	—	0.94	0.97	Sar	—	—	−0.90	−0.91	−0.88	0.77
Bet	−0.94	—	−0.80	−0.83							
L9	0.94	0.90	−0.81	—							
Act	—	0.95	−0.75	—							
Ace	—	−0.76	0.82	—							
α-Glc	—	−0.94	0.83	—							
β-Glc	—	−0.93	0.80	—							

[a] Abbreviations in tables explained in the notes of figure 2.

pyruvate. The high level of ketone bodies including acetone and acetoacetate in the urine of the dosed group also suggests that fatty acids were used as an alternative source of energy.

3.5.3. Metabonomic analysis of liver. As identified by the biodistribution results (figure 3), liver was a Mn-NP-targeted organ. Therefore, most of the endogenous metabolites in the liver changed upon Mn-NP treatment, as shown in table 3(A). Among them, the concentration changes of Ala, AMP, Tyr, dimethylamine, valine (Val), tryptophan (Trp), fumarate, 3-hydroxybutyrate, adenosine, niacinamide, trigonelline, 2-hydroxyisobutyrate, Phe, *N*-acetylglutamate (NAG), choline, Ile, GPC, GSH, phosphocholine (PC), allantoin, glycogen, oxaloacetate, glutamate (Glu), and glucose were directly correlated with Mn content. The changes of Leu, aspartate (Asp), γ-aminobutyrate (GABA), and guanosine were high-dose specific, while that of formate and propionate were low-dose specific. Pyroglutamate, betaine, acetate, lactate, Gln, uridine, Gly, uracil, succinate, NAD^+, and $NADP^+$ demonstrated a complicated effect of body response to Mn-NP exposure.

The elevation of aromatic amino acids including Trp, Tyr, and Phe has been proposed for predicting the extent of hepatic necrosis and possibly outcome [21]. The obvious increase of Trp, Tyr, and Phe in our study implies that high-dose Mn-NP exposure induced to a certain extent hepatic or splenic necrosis at 6 h pd. As a natural biological response, a detoxification process was stimulated; correspondingly, NAD(P), $FADH_2$, and their substrate niacinamide were elevated in the liver. Consistent with this result, the excretion of urinary niacin, niacinamide, and their metabolites was decreased. In addition, we noticed the levels of branched-chain amino acids (BCAAs) including Val, Leu, and Ile, as important nutrients in the detoxification process, were strongly correlated to tissue distribution of Mn-NPs in brain, liver, and spleen (table 3(A)).

Table 3. Summary of metabolic variations in (A) liver extracts induced by Mn-NPs between different pairwise groups and (B) rat tissues induced by Mn-NPs between different pairwise groups.

(A)

Metabolites	C6–L6	C6–H6	C48–L48	C48–H48	Metabolites	C6–L6	C6–H6	C48–L48	C48–H48
Ala[a]	—	0.85	—	—	OA	0.89	0.86	0.80	0.76
AMP	—	0.98	—	—	Glu	0.88	0.91	0.77	0.88
Tyr	—	0.92	—	—	β-Glc	−0.91	−0.98	−0.91	−0.86
DMA	0.82	0.85	—	—	α-Glc	−0.97	−0.99	−0.87	−0.92
Val	0.91	0.98	—	—	Leu	—	0.81	—	0.77
Trp	0.91	0.88	—	—	Asp	—	0.82	—	0.87
Fum	0.91	0.87	—	—	GABA	—	0.79	—	0.76
3-HB	0.88	0.82	—	—	Gu	—	0.85	—	0.88
Ade	0.85	0.88	—	—	For	0.97	—	0.90	—
NA	0.99	0.95	—	—	Prop	0.84	—	0.88	—
Tri	0.84	0.80	—	—	Bet	−0.76	—	—	—
2-HIB	−0.77	−0.79	—	—	Ace	—	—	0.80	—
Phe	0.97	0.99	—	0.80	Lac	—	—	—	0.78
NAG	0.92	0.95	—	0.80	Gln	—	—	—	0.90
Ch	0.89	0.94	—	0.83	Ud	—	—	—	−0.80
Ile	0.85	0.88	—	0.76	Gly	—	—	—	−0.75
GPC	0.82	0.95	—	0.86	Ura	0.82	0.89	−0.79	—
GSH	0.91	0.94	—	0.78	Suc	—	0.93	0.76	—
PC	0.78	0.88	—	0.82	PG	0.96	0.88	0.89	—
All	−0.94	−0.92	—	−0.88	NAD	−0.91	—	−0.91	0.92
Glg	−0.98	−0.98	—	−0.92	NADP	−0.89	—	−0.95	0.82

(B)

	Brain					Spleen			
Metabolites	C6–L6	C6–H6	C48–L48	C48–H48	Metabolites	C6–L6	C6–H6	C48–L48	C48–H48
Gu	—	−0.82	—	—	Tyr	—	0.84	—	—
Phe	0.79	0.91	—	0.75	Lac	—	0.95	—	—
GABA	0.93	0.96	0.79	0.76	Ile	0.86	0.78	—	—
m-I	0.99	0.97	0.84	0.83	Val	0.83	0.81	—	0.82
Ura	0.83	0.88	0.87	0.87	Phe	0.92	0.96	—	0.85
Prop	−0.85	−0.85	0.85	−0.93	Suc	0.78	0.78	0.88	0.88
Lac	0.99	0.99	—	—	Bet	—	—	−0.94	−0.95
Cr	0.99	0.98	—	—	Ala	—	—	—	0.82
Glu	0.98	0.97	—	—	EA	—	—	—	0.83
Cyt	0.85	0.77	—	—	m-I	—	—	—	0.88
Ade	0.89	0.79	—	—	NAD	—	—	—	0.95
Asp	0.81	0.88	—	—	Tau	—	—	—	−0.75
β-Glc	−0.94	−0.92	—	—	PC	—	—	—	−0.93
PEA	−0.84	−0.79	—	—	Ace	—	—	0.78	—
All	−0.95	−0.95	—	—	Cn	—	—	0.92	—
Tau	−0.85	−0.87	—	—	For	—	—	0.93	—
PC	−0.88	−0.76	—	—	α-Glc	—	—	−0.79	—
α-Glc	−0.93	−0.93	—	—	Sar	—	—	−0.71	—
Glg	−0.92	−0.93	—	—	Lys	0.80	—	—	—
Val	−0.83	−0.81	—	—	DMG	0.83	—	—	—
GPC	−0.84	−0.86	—	—	Leu	0.85	—	—	—
Thr	−0.93	−0.91	—	—	Glu	0.91	—	—	—
For	0.94	—	0.93	—	Prop	—	—	0.92	−0.78
Cn	0.97	—	0.94	—	PG	—	−0.75	0.94	—
Eth	−0.79	−0.75	−0.84	—	NA	—	0.77	0.88	—
NAD	−0.91	−0.84	−0.76	—	Cr	−0.78	—	0.77	0.83
NAA	1.00	0.99	0.76	—	Ura	0.77	0.78	−0.76	—
Suc	0.75	—	—	—					
Fum	0.84	—	—	—					
Ile	−0.81	—	—	—					
Ace	—	—	—	−0.75					
PG	0.99	—	0.88	−0.95					
Leu	−0.85	−0.84	—	0.80					

[a] Abbreviations in tables explained in the notes of figure 2.

GSH is synthesized and metabolized via the γ-glutamyl cycle. The elevated GSH levels in liver were associated with the formation of reactive metabolite in response to Mn-NP exposure. As an intermediate in the γ-glutamyl cycle, the high level of pyroglutamate in brain, liver, lung, and spleen tissues suggests that more GSH was needed for detoxification. Besides, when cystathionine is converted to cysteine and incorporated into GSH, 2-hydroxybutyrate is released and excreted into urine (table 2).

Urea production occurs primarily in the liver. Carbamoyl phosphate synthetase I is essential for urea synthesis, while its activity is absolutely dependent on NAG, which is synthesized from acetyl-CoA and Glu. Our results show that the variation of NAG content was correlated with Mn content in the liver. This suggests that Mn-NPs promoted amino acid catabolism. Besides, the alternation of fumarate, oxaloacetate, Gln, Glu, and Asp levels may also be related to the nitrogen metabolism.

Catabolism of putrescine, one of the polyamines, occurs along different pathways, but GABA is as a common intermediate. *S*-adenosylmethionine is the principal methyl donor and precursor for polyamines. Though the function of polyamines is not entirely clear, they play an essential role in promoting cell growth and hepatic regeneration. Thus an increase of GABA concentration in high-dose groups could imply the regeneration of hepatic injury induced by Mn-NP administration.

Choline-like metabolites such as choline, PC, and GPC take part in several important biochemical pathways, including a signaling and structural role for cell membranes and an immune response regulator. Previous studies have shown that PC bound to C-reactive protein, subsequently activated complement, and began the phagocytotic immunologic response [22]. So it is possible that elevated levels of these metabolites help to remove the damaged liver cells.

3.5.4. Metabonomic analysis of brain. In brain homogenates, guanosine, Phe, GABA, *myo*-inositol, uracil, and propionate may be related to the Mn content in the brain. The levels of lactate, creatine, Glu, cytidine, adenosine, Asp, glucose, *O*-phosphoethanolamine, allantoin, taurine, PC, glycogen, Val, GPC, and Thr were changed in a time-dependent manner (table 3(B)). The alteration of formate and Cn were specific in the low-dose group. However, the succinate, fumarate, Ile, acetate, ethanol, NAD^+, and *N*-acetylaspartate (NAA) levels were changed in a complicated manner.

Three intermediates of the GABA shunt (in which the inhibitory neurotransmitter GABA is synthesized and degraded), GABA, Glu, and succinate, were increased in brain tissue at 6 h pd. Previous studies revealed that Mn exposure inhibited the synthesis and release of glutamine [23]. Moreover, creatine and Cn served as indicators of brain energy metabolism in depression [24]. Whether the increased level of these metabolites caused mental depression in rats is unclear. However, Mn-NP exposure influenced neurotransmission, which might affect the brain energy metabolism in rats.

Consistent with the result of plasma, Mn-NP exposure caused an increase in the oxygen consumption, and stimulated anaerobic glycolysis, which may be responsible for the increased level of lactate and the decreased levels of glucose and glycogen in brain, lung, and spleen samples (table 3(B)). Under anaerobic conditions, formate, acetate, fumarate, and succinate were produced and in the presence of citrate with the reaction: 2 lactate + 1 citrate $\rightarrow$ 3 acetate + 2 formate + 1 fumarate (the ensuing reduction of fumarate to succinate). Lactate is further reduced to propionate, and acetyl-CoA can be reduced to ethanol. In addition, as an important fuel source, the levels of BCAAs were decreased with increased energy consumption at 6 h pd. This conclusion was supported by the increased urinary 2-oxoisovalerate (an intermediate in the BCAA catabolic pathway). In addition, NAA is synthesized in the mitochondria of neurons from Asp and acetyl-CoA. One possible physiological role for NAA is in adjusting the intracellular osmolarity, together with *myo*-inositol, GPC, and taurine.

A comprehensive difference in metabolic profiles was also observed with time in the control groups (data not shown), which included an increase of GABA, lactate, creatine, Glu, Cn, and NAA and a decrease of *O*-phosphoethanolamine, allantoin, taurine, PC, glucose, glycogen, Val, GPC, Thr, NAD^+, and Leu at 48 h pd. Previous studies have shown that the stress of normal intravenous injection caused release of stress hormones in a time-dependent manner. Although there is no evidence that the restraint stress can affect the Mn ion distribution, the toxic effects of Mn-NPs may be more obvious in a stressful situation [25]. We assume that the restraint stress would enhance the neurotoxic effects of Mn-NP exposure on global metabolite profiles; however, these effects on the brain could be transient and recoverable (figure 3 and table 3(B)).

3.5.5. Metabonomic analysis of spleen. In spleen homogenates, the alterations of Tyr, lactate, Ile, Val, Phe, and succinate were dependent on Mn biodistribution in the spleen, while the change of betaine was time dependent. The other metabolites, such as Ala, ethanolamine, *myo*-inositol, NAD^+, taurine, PC, acetate, Cn, formate, glucose, sarcosine, Lys, dimethylamine, Leu, Glu, propionate, pyroglutamate, niacinamide, creatine, and uracil were changed in a complicated manner (table 3(B)).

Previous evidence has shown that excessive Mn inhibited the activity of succinic dehydrogenase [26], which led to increased succinate levels in spleen. PC and ethanolamine are components for the synthesis of phospholipids. *Myo*-inositol is a secondary messenger in the PI3K/Akt signaling pathway and an intracellular organic osmolyte. Taurine is involved in many physiological processes, including osmoregulation, toxic intermediate clearance, and calcium mobilization [27]. Ala is one of the most abundant amino acids in the body, it can be easily synthesized from pyruvate and BCAAs, and it is extensively used as an intermediate in many metabolic pathways such as glycolysis, gluconeogenesis, tricarboxylic acid cycle, and Ala cycle. High niacinamide could help the spleen detoxify Mn-NPs, which also took place in the liver, lung, and kidney. Creatine is naturally produced in the body from amino acids and dehydrated to form the cyclic shift base

Cn in rat heart, spleen, and skeletal muscle and excreted by kidney. Relatively speaking, among all observed tissues, the metabolic profile of spleen was less affected by Mn-NPs.

3.5.6. Metabonomic analysis of kidney and lung. Mn-NPs induced weaker effects on kidney and lung, and metabolic variations seem to be closely correlated with the blood clearance and the biodistribution of Mn-NPs as identified by ICP-AES (figure 3). Time-dependent changes were observed in the levels of betaine, uracil, *myo*-inositol, GPC, Glu, Val, pantothenate, and Tyr in the renal metabonome, while succinate, lactate, cytidine, Glu, uracil, glycogen, and glucose were changed in a Mn content-dependent manner in the lung metabonome (table S2 available at stacks.iop.org/Nano/24/455102/mmedia). Betaine, *myo*-inositol, GPC, and Glu help osmoregulate the extracellular osmolality, and the changes in the levels of succinate, betaine, choline, and Glu seem to be related to the detoxification process in response to Mn-NP exposure [28]. As important intermediates of fatty acid, protein, and RNA synthesis, the variations of pantothenate, Phe, cytidine, uracil, Val, and Tyr implied the disturbance of the related metabolic pathways induced by Mn-NP treatment.

According to our results, exposure to Mn-NPs had effects on a number of metabolic pathways including energy, lipid, amino acid, and other nutrient metabolism in rats. Furthermore, the information of absorption, transportation, biodistribution, and excretion could be derived from the variations of the metabolites in the specific tissues. However, the disturbance and impairments of biological functions induced by nanoparticles are closely correlated with the particle size and surface chemistry [13, 29]. Therefore, it is feasible to improve their biocompatibility and safety profiles by optimizing the particle size and modifying the surface structure when Mn-NPs are used as MRI contrast agents.

4. Conclusions

Exposure to Mn-NPs could lead to disturbances of a number of metabolic processes in the organism. However, the detoxification system *in vivo* is so complex and influenced by so many regulatory mechanisms that no single technology can fulfil complete analyses. In this study, we integrated the traditional biochemical analyses with NMR-based metabonomics as a systematic approach to investigate the toxicological effects of *in vivo* exposures to Mn-NPs. The dysfunction induced by Mn-NPs was demonstrated as variations of all kinds of metabolite in specific tissues. The removal of nanoparticles from the body is a biochemical process known as detoxification or metabolism. As an important factor in ADME, the detoxification process directly affects distribution and excretion. In addition, the biocompatibility and safety profiles could be improved by optimizing the particle size and modifying the surface structure when Mn-NPs are used as MRI contrast agents. Our results suggest that NMR-based metabonomic analysis is a suitable approach for evaluating the ADME/Tox properties of Mn-NPs in contrast agent development, which would provide identifiable ground for candidate selection and optimization.

Acknowledgments

We acknowledge financial support from the National Natural Science Foundation of China (20605025, 81272581) and the Fundamental Research Funds for the Central Universities (2011121046).

References

[1] Nordhoy W, Anthonsen H W, Bruvold M, Brurok H, Skarra S, Krane J and Jynge P 2004 Intracellular manganese ions provide strong T1 relaxation in rat myocardium *Magn. Reson. Med.* **52** 506–14
[2] Lelyveld V S, Brustad E, Arnold F H and Jasanoff A 2011 Metal-substituted protein MRI contrast agents engineered for enhanced relaxivity and ligand sensitivity *J. Am. Chem. Soc.* **133** 649–51
[3] Kirchin M A and Runge V M 2003 Contrast agents for magnetic resonance imaging: safety update *Top. Magn. Reson. Imag.* **14** 426–35
[4] Crossgrove J and Zheng W 2004 Manganese toxicity upon overexposure *NMR Biomed.* **17** 544–53
[5] Schladt T D *et al* 2010 Highly soluble multifunctional MnO nanoparticles for simultaneous optical and MRI imaging and cancer treatment using photodynamic therapy *J. Mater. Chem.* **20** 8297
[6] Na H B *et al* 2007 Development of a T1 contrast agent for magnetic resonance imaging using MnO nanoparticles *Angew. Chem. Int. Edn* **46** 5397–401
[7] Huang C C, Khu N H and Yeh C S 2010 The characteristics of sub 10 nm manganese oxide T1 contrast agents of different nanostructured morphologies *Biomaterials* **31** 4073–8
[8] Pellegatti M 2012 Preclinical *in vivo* ADME studies in drug development: a critical review *Expert Opin. Drug Metab. Toxicol.* **8** 161–72
[9] Nicholson J K, Connelly J, Lindon J C and Holmes E 2002 Metabonomics: a platform for studying drug toxicity and gene function *Nature Rev. Drug Discov.* **1** 153–61
[10] Duarte I F 2011 Following dynamic biological processes through NMR-based metabonomics: a new tool in nanomedicine? *J. Control. Release* **153** 34–9
[11] Schladt T D, Graf T and Tremel W 2009 Synthesis and characterization of monodisperse manganese oxide nanoparticles-evaluation of the nucleation and growth mechanism *Chem. Mater.* **21** 3183–90
[12] Wu H, Southam A D, Hines A and Viant M R 2008 High-throughput tissue extraction protocol for NMR- and MS-based metabolomics *Anal. Biochem.* **372** 204–12
[13] Feng J, Liu H, Bhakoo K K, Lu L and Chen Z 2011 A metabonomic analysis of organ specific response to USPIO administration *Biomaterials* **32** 6558–69
[14] Moghimi S M, Hunter A C and Andresen T L 2012 Factors controlling nanoparticle pharmacokinetics: an integrated analysis and perspective *Annu. Rev. Pharmacol. Toxicol.* **52** 481–503
[15] Breslow R, Huang Y, Zhang X and Yang J 1997 An artificial cytochrome P450 that hydroxylates unactivated carbons with regio-and stereoselectivity and useful catalytic turnovers *Proc. Natl Acad. Sci.* **94** 11156–8
[16] Akoume M Y, Perwaiz S, Yousef I M and Plaa G L 2003 Synergistic role of 3-hydroxy-3-methylglutaryl coenzyme a reductase and cholesterol 7alpha-hydroxylase in the pathogenesis of manganese–bilirubin-induced cholestasis in rats *Toxicol. Sci.* **73** 378–85
[17] Feng J, Liu H, Zhang L, Bhakoo K and Lu L 2010 An insight into the metabolic responses of ultra-small superparamagnetic particles of iron oxide using

metabonomic analysis of biofluids *Nanotechnology* **21** 395101
[18] Lenney J F 1990 Separation and characterization of two carnosine-splitting cytosolic dipeptidases from hog kidney (carnosinase and non-specific dipeptidase) *Biol. Chem. Hoppe–Seyler* **371** 433–40
[19] Chlopicki S, Swies J, Mogielnicki A, Buczko W, Bartus M, Lomnicka M, Adamus J and Gebicki J 2007 1-Methylnicotinamide (MNA), a primary metabolite of nicotinamide, exerts anti-thrombotic activity mediated by a cyclooxygenase-2/prostacyclin pathway *Br. J. Pharmacol.* **152** 230–9
[20] Espinós C, Pineda M, Martínez-Rubio D, Lupo V, Ormazabal A, Vilaseca M A, Spaapen L J, Palau F and Artuch R 2009 Mutations in the urocanase gene UROC1 are associated with urocanic aciduria *J. Med. Genet.* **46** 407–11
[21] Bernardini P and Fischer J E 1982 Amino acid imbalance and hepatic encephalopathy *Annu. Rev. Nutr.* **2** 419–54
[22] Thompson D, Pepys M B and Wood S P 1999 The physiological structure of human C-reactive protein and its complex with phosphocholine *Structure* **7** 169–77
[23] Burton N C, Schneider J S, Syversen T and Guilarte T R 2009 Effects of chronic manganese exposure on glutamatergic and GABAergic neurotransmitter markers in the nonhuman primate brain *Toxicol. Sci.* **111** 131–9
[24] Della F P *et al* 2012 Tianeptine treatment induces antidepressive-like effects and alters BDNF and energy metabolism in the brain of rats *Behav. Brain Res.* **233** 526–35
[25] Chandra S V, Shukla G S and Murthy R C 1979 Effect of stress on the response of rat brain to manganese *Toxicol. Appl. Pharmacol.* **47** 603–8
[26] Bhadauria M, Nirala S K and Shukla S 2007 Duration-dependent hepatoprotective effects of propolis extract against carbon tetrachloride-induced acute liver damage in rats *Adv. Ther.* **24** 1136–45
[27] Boşgelmez II, Söylemezoğlu T and Güvendik G 2008 The protective and antidotal effects of taurine on hexavalent chromium-induced oxidative stress in mice liver tissue *Biol. Trace Elem. Res.* **125** 46–58
[28] Wang M, Luo Z, Liu S, Li L, Deng X, Huang F, Shang L, Jian C and Yue S 2009 Glutamate mediates hyperoxia-induced newborn rat lung injury through *N*-methyl-D-aspartate receptors *Am. J. Respir. Cell Mol. Biol.* **40** 260
[29] Mahajan S, Koul V, Choudhary V, Shishodia G and Bharti A C 2013 Preparation and *in vitro* evaluation of folate-receptor-targeted SPION-polymer micelle hybrids for MRI contrast enhancement in cancer imaging *Nanotechnology* **24** 015603